Supplementary information

Analytical Techniques and Measurement Uncertainty

Interferomeric SAR (InSAR) allows measurement of millimetre-level surface displacements, including land subsidence, in the radar illumination direction[1-10]. This is accomplished by phase comparison of two or more images separated in time. Apart from cycle ambiguity problems, the main limitations are related to temporal and geometrical decorrelation (low signal to noise ratio in the phase change estimate), and variable tropospheric water vapor, which can generate variable path delay for microwave signals unrelated to surface motions. In sub-tropical and tropical regions, the tropospheric delay may be as high as 10 cm over several weeks [11-12]. This constitutes a significant potential error source for InSAR, and has tended to restrict most InSAR studies to relatively dry regions. Permanent Scatterer InSAR (PSInSAR)[13-18] exploits several characteristics of radar scattering and atmospheric decorrelation to measure surface displacement in otherwise non-optimum conditions, including humid regions. Atmospheric phase contributions are spatially correlated within a single SAR scene, but are generally uncorrelated in time. Conversely, target motion is usually strongly correlated in time. Thus, atmospheric effects can be estimated and removed by combining data from long time series of SAR images, in effect averaging the temporal fluctuations. Scatterers that are only slightly affected by temporal and geometrical decorrelation are used, allowing exploitation of all available images regardless of imaging geometry. In this sense the scatterers are "permanent", i.e., persistent over many satellite revolutions. Inspection of the individual points indicates that many of the scatterers are located at the intersection of a street or sidewalk and vertical structure such as the side of a building, or a roof (Figure S-1). Parks and other vegetated areas in contrast have no or few permanent scatterers.

The interferograms have a common time reference (master acquisition) allowing a first order precision assessment. The *a posteriori* standard deviation is computed based on one or more ground control points of known elevation and motion[16,19] (Figure S-2).

We used 33 RADARSAT (6 cm wavelength) scenes acquired between April 2002 and July 2005 in the ascending orbit, standard beam mode S-2. We focused on greater New Orleans, where urbanization provides a number of well-defined radar targets. A total of more than 1.8×10^5 radar targets were identified in this region that retained some phase coherence over the three year study period. Of these, $\sim 3.9 \times 10^4$ targets had coherence in excess of 0.6, and $\sim 3.1 \times 10^4$ targets had coherence in excess of 0.8, providing excellent phase fidelity and spatial resolution for our space-derived surface velocity map. The mean and standard deviation range change rate for all the point targets is -5.6±2.5 mm/yr. Using just the point targets where coherence is greater than 0.9, the corresponding rate and standard deviation is essentially identical, -5.4±2.2 mm/yr.

For permanent scatterer interferometry, the phase history contributions from elevation (scatterer height) and motion must be separated. However, depending on the baseline distribution of the SAR scenes, there may be a residual correlation between height and

motion that makes the separation difficult, such that high subsidence rates might be wrongly estimated as high scatterer elevations. In our approach, the contributions to interferometric phase due to motion and topography are estimated jointly. This step can be considered as the estimation of the frequency of a two-dimensional complex sinusoid, where the axes of the two-dimensional space are represented by time of acquisition and the baseline normal vector. If these two dimensions are orthogonal (i.e., there is no correlation between time and the baseline normal), there is no risk that a contribution due to velocity can be misinterpreted as topography. For the New Orleans data, the correlation coefficient between the time of acquisition and the baseline normal is very small, 0.0400, indicating that the orthogonality condition is satisfied. Thus it is highly unlikely that high subsidence rates are incorrectly interpreted as higher scatterer elevations.

Interferometric measurements by definition are relative (ambiguous), hence determination of subsidence requires calibration with one or more ground control points of known elevation and motion. This is usually accomplished by referencing to stable areas ~50 km away from the locus of deformation, where motions are assumed to be minimal. This is problematic in the Gulf coast, where a large region is thought to be subsiding. We use a ten year time series from a high precision GPS station in the greater New Orleans area (ENG1) to provide an independent reference. A nearby site (ENG2) with a shorter time series gives an essentially identical result. The data are analyzed in such a way that the vertical position component may be considered "absolute" i.e., referenced to the International Terrestrial Reference Frame (ITRF), ultimately related to Earth center of mass[20]. The surface velocity map (Figure 1) is referenced to this GPS "datum".

For the 33 RADARSAT scenes in this study, the *a posteriori* standard deviation in rate is better than 2.5 mm/yr for 90% of the scatterers. The rate uncertainty is a function of the total time span of observations, the number of data, and the "white" (uncorrelated) and time-correlated noise for the individual time series[21]. The individual time series (Figure S-3) for the most part are consistent with steady motion over the three year observation period, but do exhibit some time-correlated noise[22,23] which may reflect the residual influence of atmospheric or satellite orbit variations, as well as systematic surface and sub-surface processes, some of which could have an annual period. Natural annual recharge of sub-surface acquifers and episodic fluid withdrawal are therefore potential error sources, given our assumption of a constant rate of range change. However, large scale fluid withdrawal in the region ceased more than a decade prior to our first measurements, and thus should not significantly influence our results. Inspection of the time series for individual permanent scatterers suggests that annual variation is small for most of them, compared to the longer term secular trend (Figure S-3).

 The total uncertainty of the subsidence estimate is the *rss (*root sum square*)* of the *a posteriori* standard deviation and the uncertainty of the GPS datum itself, 1.0 mm/yr (one sigma). The latter value is sufficiently small that it can be ignored. Assuming purely vertical motion, the subsidence rate is $\rho/\cos\alpha$, where ρ and α are the range change and incidence angle (from vertical) of the radar, respectively. For a 29° incidence angle (the

approximate angle for RADARSAT standard beam mode 2 at the center of the New Orleans scene) -10.0 mm/yr range change is equivalent to about 11.4 mm/yr of subsidence; the difference is close to the standard deviation of the measurements (Figure S-2).

The uncertainty of our subsidence measurements is related to the distance of a permanent scatterer to the GPS calibration point (Figure S-2). For the MRGO levee scatterers, this distance is relatively short (< 15 km), and the corresponding total uncertainty is less than 2.0 mm/yr, much less than the ~ 20 mm/yr or greater subsidence rates we measure. Hence, the high subsdidence rates that we measure, as well as the correlation with levee breaches on the MRGO levee (Figure S-4), is robust.

References for supplementary information

1. Massonnet, D. & Feigl, K. Radar interferometry and its application to changes in the Earth's surface. *Rev. Geophys.* **36**, 441-500 (1998).

2. Rosen, P.A. et al.; Synthetic aperture radar interferometry. *Proc. IEEE* **88**(3), 333-382 (2000).

3. Hanssen, R.F., Radar Interferometry, Kluwer Academic Publishers (2001).

4. Massonnet, D., Holzer, T. & Vadon, H. Land subsidence cause by East Mesa geothermal field, California, observed using SAR interferometry, *Geophys. Res. Lett.* **24**, 901-904 (1997).

5. Galloway, D. L., Hudnut, K. W., Ingebritsen, S. E., Phillips, S. P., Pelzer, G., Rogez, F. , & Rosen, P. A. InSAR detection of system compaction and land subsidence, Antelope Valley, Mojave Desert, California. *Water Resources Res.* **34**, 2573-2585 (1998).

6. Fielding, E. J., Blom, R. G., & Goldstein, R. M. Rapid subsidence over oil fields measured by SAR interferometry. *Geophys. Res. Lett.* **25**, 3215-3219 (1998).

7. Amelung, F., Galloway, D. L., Bell, J. W., Zebker, H. A. & Laczniak, R. J. Sensing the ups and downs of Las Vegas: InSAR reveals structural control of land subsidence and acquifer system deformation. *Geology 27*, 483-486 (1999).

8. Bawden, G. W., Thatcher, W., Stein, R. S., Hudnut, K. W. & Peltzer, G. Tectonic contraction across Los Angeles after removal of groundwater pumping effects. *Nature* **412**, 812-815 (2001).

9. Buckley, S.M., Rosen, P.A., Hensley, S. & Tapley, B.D., Land subsidence in Houston, Texas, measured by radar interferometry and constrained by extensometers. *J. Geophys. Res.*-Solid Earth **108**(B11) (2003).

10. Tesauro, M. et al. Urban subsidence inside the city of Napoli (Italy) observed by satellite radar interferometry. *Geophys. Res. Lett* **27**(13): 1961-1964 (2000).

11. Dixon, T. H. & Kornreich Wolf, S. Some tests of wet tropospheric calibration for the CASA UNO Global Positioning System experiment. *Geophys. Res. Lett.* **17**, p.203-206 (1990).

12. Dixon, T. H., Gonzalez, G., Lichten, S. & Katsigris, E. First epoch geodetic measurements with the Global Positioning System across the northern Caribbean plate boundary zone. *J. Geophys. Res.* **96**, 2397-2415 (1991).

13. Ferretti, F., Prati, C. & Rocca, F. Nonlinear subsidence rate estimation using permanent scatterers in differential SAR Interferometry. *IEEE Trans. Geoscience Remote Sensing* **38**(5), 2202-2212 (2000).

14. Ferretti, F., Prati, C. & Rocca, F. Permanent scatterers in SAR Interferometry. *IEEE Trans. Geosci. Remote Sensing*, **39**(1), 8-20 (2001).

15. Colesanti, C., Ferretti, A., Novali, F., Prati, C. & Rocca, F. SAR monitoring of progressive and seasonal ground deformation using the permanent scatterers technique. *IEEE Trans. Geosci. Remote Sensing*, **41**(7), 1685-1701 (2003a).

16. Colesanti, C., Ferretti, A., Prati, C. & Rocca, F. Monitoring landslides and tectonic motions with the permanent scatterer technique, *Engineering Geol., Spec. Issue Remote Sensing and Monitoring of Landslides,* **68**(1), 3-14 (2003b).

17. Hilley, G. E., Burgmann, R., Ferretti, A., Novali, F. & Rocca, F. Dynamics of slow-moving landslides from permanent scatterer analysis. *Science* **304**, 1952-1955 (2004).

18. Ferretti, A., Novali, F., Burgmann, R., Hilley, G. & Prati, C. InSAR Permanent Scatterer analysis reveals ups and downs in San Francisco Bay area. *EOS*, **85**(34), 1-3 (2004).

19. Colesanti, C., Ferretti, A., Locatelli, R., Novali, F. & Savio, G. Permanent scatterers: precision assessment and multi-platform analysis. *Int. Geosci. Remote Sensing Symp.*, Tolouse, France (2003c).

20. Analytical details and a discussion of the reference frame are given in Sella, G., Dixon, T. H. & Mao, A. REVEL: a model for Recent plate velocities from space geodesy. *J. Geophys. Res.* **107**, B4, 10.1029/2000JB000033 (2002).

21. See for example Mao, A., Harrison, C.G.A. & Dixon, T. H. Noise in GPS coordinate time series. *J. Geophys. Res.* **104**, 2797 – 2816 (1999).

22. Johnson, H. O. & Agnew, D. C. Monument motion and measurement of crustal velocity. *Geophys. Res. Lett.* 22, 2905-2908 (1995).

23. Langbein, J. & Johnson, H. Correlated errors in geodetic time series: implications for time dependent deformation. *J. Geophys. Res.*, **102**, 591-604 (1997).

24. *Response to Hurricanes Katrina and Rita in Louisiana* Environmental Assessment 433 (US Army Corps of Engineers, 2006).
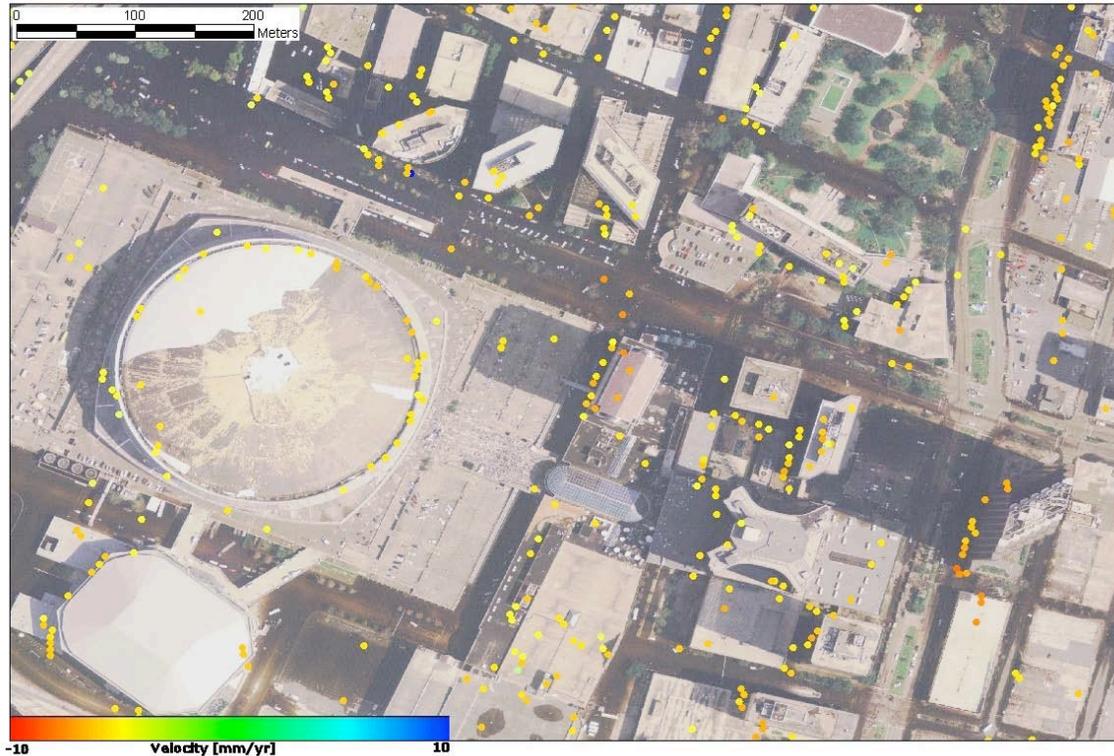
Supplementary figures

Figure S1. Close up of Superdome near downtown New Orleans from aerial photography after Hurricane Katrina (note damaged roof of Superdome), with superimposed velocity of permanent scatterers. Radar illumination from left, solar illumination from right.
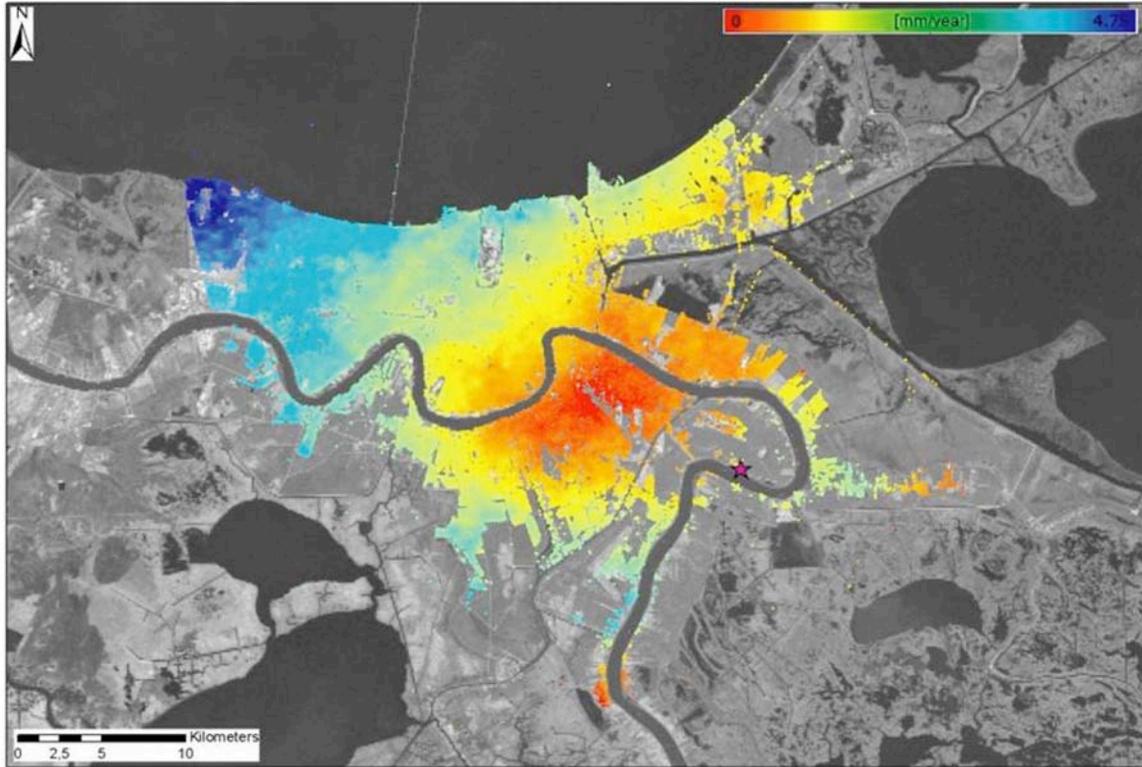

Figure S2. Standard deviation of individual permanent scatterers. Star marks location of GPS calibration point ENG1.
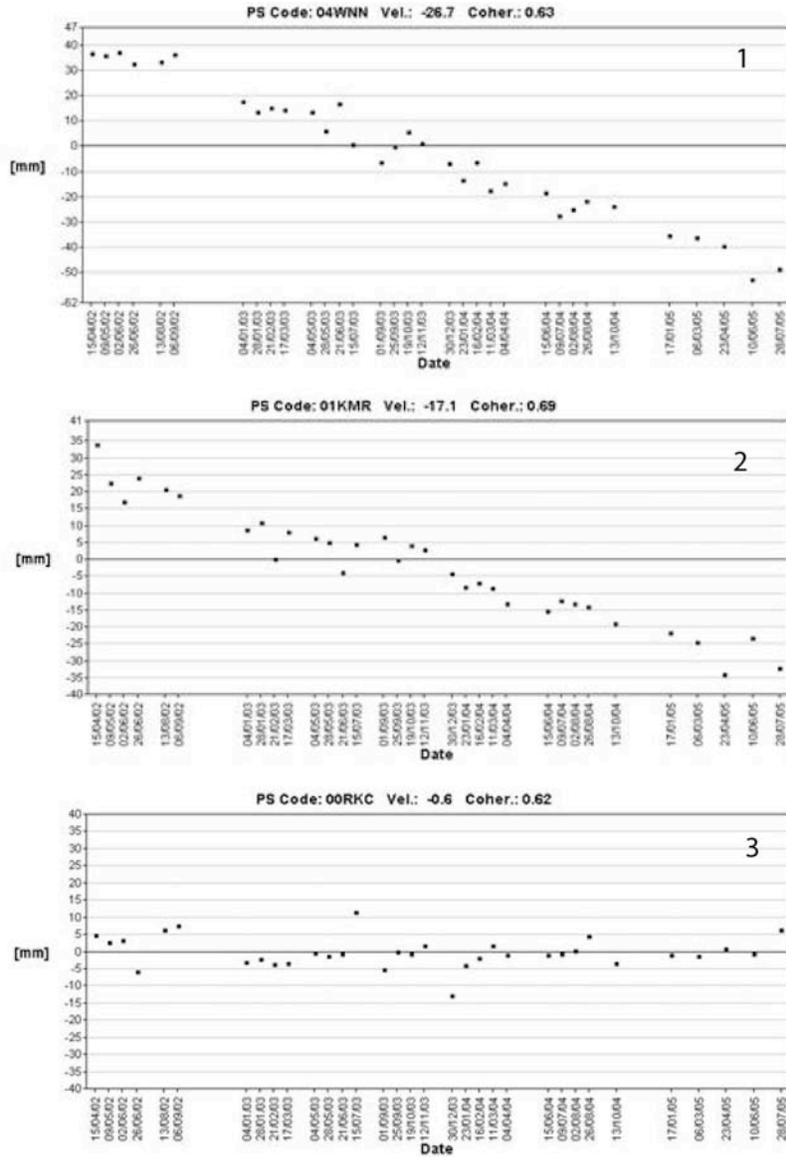
Figure S3. Time series of several individual permanent scatterers. Each point represents data for an individual pixel from an individual SAR image (total 33). Points 1 and 2 are on the levee bounding the MRGO canal, point 3 is within 1 km of the GPS calibration point.

Figure S4. Map of breached levees in St Bernard Parish[24]. Note breached levees along MRGO, corresponding to high subsidence rates (Figure 1, inset).